Archives of Acoustics Vol. 46, No. 4, pp. 637–647 (2021), doi: 10.24425/aoa.2021.139640

Research Paper

Influence of Geometric Structure, Convection, and Eddy on Sound Propagation in Acoustic Metamaterials with Turbulent Flow

Myong Chol PAK(1)*, Kwang-Il KIM(1), Hak Chol PAK(1), Kwon Ryong HONG(2)

(1) *Department of Physics, Kim Il Sung University*
Taesong District, Pyongyang, Democratic People's Republic of Korea
*Corresponding Author e-mail: myongcholpak@163.com

(2) *Institute of Natural Sciences, Kim Il Sung University*
Taesong District, Pyongyang, Democratic People's Republic of Korea

(*received April 21, 2021; accepted September 28, 2021*)

The problem of reducing noise in transportation is an important research field to prevent accidents and to provide a civilised environment for people. A material that has recently attracted attention in research to reduce noise is acoustic metamaterial, and most of the research projects so far have been limited to the case of static media without flow. We have studied the sound transmission properties of the acoustic metamaterials with turbulent flow to develop the acoustic metamaterials that are used in transportation. In this paper, the effects of geometrical structure, convection, and eddy on sound propagation in the acoustic metamaterials with turbulent flow are investigated, and the relationships between them are analysed. The effects of convection and eddy reduce the resonant strength of the sound transmission loss resulting from the unique geometry of the acoustic metamaterials, but move the resonant frequencies to opposite directions. In addition, when the convective effect and the eddy effect of the airflow, as well as the intrinsic interaction effect generated from the unique geometrical structure of the acoustic metamaterials cannot be ignored, they exhibit competition phenomena with each other, resulting in a widening of the resonance peak. As a result, these three effects cause the shift of the resonance frequency of the sound transmission loss and the widening of the resonance peak. The results of this study show that even in the case of turbulent flow, the metamaterials can be used for transportation by properly controlling its geometric size and shape.

Keywords: acoustic metamaterial; turbulent flow; sound transmission loss; eddy; transportation.

1. Introduction

With the recent development of technology, attention has been focused on the improvement of the human environment, and interest in noise reduction is increasing. Among others, the acoustic metamaterials is widely applied because they can reduce noise by controlling the density and the bulk modulus of the material.

Studies have been discussed using the acoustic metamaterials to control sound transmission by absorbing low-frequency sound in linear and nonlinear regions (Brookea *et al.*, 2020; Li, Assouar, 2016) and doping impurities inside zero-index metamaterials (Gu *et al.*, 2020). Moreover, the method for minimising indoor sound energy by using an acoustic metamaterial with a flat panel structure (Qu, Sheng, 2020) and the method for detecting an acoustic image by constructing an acoustic superlens using membrane-based two-dimensional metamaterial with a negative density was reported (Park *et al.*, 2015). In addition, a non-resonant metasurface design for broadband elastic wave mode division that is used for elastic communication and biomedical diagnostic evaluation has also been proposed (Zheng *et al.*, 2020). Lu *et al.* (2016) showed through simulation that the acoustic metamaterials with honeycomb structure effectively caused acoustic transmission loss in the low frequency range, and Fan *et al.* (2015) proved that the plates with circular holes blocked by membranes are effective in

sound insulation at low frequencies by using numerical analysis. Wang *et al.* (2016) proposed that a sound insulation effect can be obtained in the low frequency range by controlling the shape, stiffness, and position of a thin film-type acoustic metamaterial with a stick fixed in the middle of the frame. Acoustic metamaterials used to block broadband noise including low-frequency regions in the air can be applied to water as well as air. Bok *et al.* (2018) proposed a way to use the acoustic metasurface consisting of a membrane and an air cavity filled with meta-atoms to increase the acoustic sensitivity in water.

As the practical applicability of the acoustic metamaterial increases, research projects on acoustic metamaterial panels that can increase the noise reduction function while passing through a fluid are in active development (Jiang *et al.*, 2017; Su *et al.*, 2014; Sui *et al.*, 2015). Jung, Kim, and Lee (2018) report the design of an acoustic metamaterial panel that does not interfere with the flow of fluid while reducing the noise in a broadband in the audible frequency range. The proposed acoustic metamaterial panel allows the fluid to pass through the straight hole, but serves to block broadband noise by periodic annular cavities surrounding the hole. However, in these papers, the effect of the flow velocity of the fluid passing through the acoustic metamaterials on the sound wave is not discussed.

Meanwhile, research projects to control sound wave propagation in laminar and turbulent flows of fluids also attract attention. Yang *et al.* (2015) proposed the idea that sound waves can propagate in one direction along the surface regardless of the presence of defects or obstacles in the acoustic structure with laminar circulation flow. Research projects for investigating sound propagation properties in turbulent flow rather than laminar flow attract much attention because they have a lot to do with practical applications (Szöke *et al.*, 2020; 2018). Turbulence effect of the fuselage on the fan noise of the BLI (Boundary-Layer Ingestion) configuration (Romani *et al.*, 2020), the relationship between the structural flexibility of the elastic trailing edge and the aeroacoustic response (Nardini *et al.*, 2020), prediction of broadband sound generated in a low Mach number turbulent boundary layer by LBM (lattice Boltzmann method) (Kusano *et al.*, 2020), simulation of indoor noise generated by indoor window vibration (Wang *et al.*, 2019; Yao, Davidson, 2019), and acoustic source model to reduce aerodynamic noise generated from wind turbine blades (Tang *et al.*, 2019) have been discussed. Most of interest, such as the reduction of aerofoil interaction noise by the new serration profile groups (Carpio *et al.*, 2019; Chaitanya *et al.*, 2020), the noise generation mechanism of the controlled diffusion aerofoils and their dependence on Mach number (Deuse, Sandberg, 2020), and the role of the porous material placed on the tail edge of the 3D chamber airfoil (Ananthan *et al.*, 2020) is focused on the reduction of noise caused by the interaction between aerofoil and turbulent flow.

Most of the researchers are only interested in sound wave control and noise generation in turbulent flows, but there are few studies on the effects of geometric structure, convection, and eddy on sound propagation in the acoustic metamaterials with turbulent flow. Therefore, we discuss the effects of convection and eddy on acoustic propagation as turbulence flows into the acoustic metamaterials consisting of straight holes and periodic annular cavities surrounding the hole. Additionally, in this case, the change in broadband acoustic shielding properties according to the geometric size and the number of annular cavities is investigated. This paper is organised as follows. Section 2 describes the theoretical basis for aeroacoustic properties in turbulent flows. In Sec. 3, the numerical results of sound transmission loss and sound pressure level of the acoustic metamaterials are shown and analysed in both cases of no flow and turbulent flow. In particular, the turbulence flowing in the acoustic metamaterial is analysed by CFD (computational fluid dynamics), and based on the results, the effects of convection and eddy on sound transmission are discussed. Furthermore, the sound transmission properties according to the geometric size of the acoustic metamaterial and the number of ring-shaped cavities are also considered. Finally, in Sec. 4, the influence of geometric structure, convection, and eddy on sound propagation in the acoustic metamaterials with turbulent flows are concluded, and future application prospects are described.

2. Theoretical background

Using the linearised Navier-Stokes equation, we investigate the propagation properties of sound waves in a fluid. This equation consists of the continuity, momentum, and energy equations (Ostashev, Wilson, 2016)

$$\frac{\partial \rho_t}{\partial t} + \nabla \cdot (\rho_0 \mathbf{u}_t + \rho_t \mathbf{u}_0) = M, \tag{1}$$

$$\rho_0 \left[\frac{\partial \mathbf{u}_t}{\partial t} + (\mathbf{u}_t \cdot \nabla)\mathbf{u}_0 + (\mathbf{u}_0 \cdot \nabla)\mathbf{u}_t \right] + \rho_t (\mathbf{u}_0 \cdot \nabla)\mathbf{u}_0 = \nabla \cdot \sigma + \mathbf{F} - \mathbf{u}_0 M, \tag{2}$$

$$\rho_0 C_p \left[\frac{\partial T_t}{\partial t} + (\mathbf{u}_t \cdot \nabla)T_0 + (\mathbf{u}_0 \cdot \nabla)T_t \right] + \rho_t C_p (\mathbf{u}_0 \cdot \nabla)T_0 - \alpha_p T_0 \left[\frac{\partial p_t}{\partial t} + (\mathbf{u}_t \cdot \nabla)p_0 + (\mathbf{u}_0 \cdot \nabla)p_t \right] - \alpha_p T_t (\mathbf{u}_0 \cdot \nabla)p_0 = \nabla \cdot (\kappa \nabla T_t) + \Phi + Q, \tag{3}$$

where p_t, $\mathbf{u}_t$, T_t, and ρ_t are the acoustic perturbations to the pressure, velocity, temperature, and density, respectively. The viscous dissipation function Φ is defined by Eq. (7). p_t, $\mathbf{u}_t$, and T_t are equal to the sum of the physical quantities in the background acoustic field and the scattered field

$$p_t = p + p_b, \quad \mathbf{u}_t = \mathbf{u} + \mathbf{u}_b, \quad T_t = T + T_b. \tag{4}$$

Also, M, $\mathbf{F}$, Q, C_p, α_p, and κ are the mass source, the volume force source, the volumetric heat source, the heat capacity at constant pressure, the coefficient of thermal expansion, and the thermal conductivity, respectively. Additionally, the stress tensor, the linearised equation of state, and the linearised viscous dissipation function are defined as

$$\sigma = -p_t\mathbf{I} + \mu\left[\nabla\mathbf{u}_t + (\nabla\mathbf{u}_t)^{\mathrm{T}}\right] + \left(\mu_B - \frac{2}{3}\mu\right)(\nabla\cdot\mathbf{u}_t)\mathrm{I}, \tag{5}$$

$$\rho_t = \rho_0(\beta_T p_t - \alpha_p T_t), \tag{6}$$

$$\Phi = \nabla\mathbf{u}_t : \tau(\mathbf{u}_0) + \nabla\mathbf{u}_0 : \tau(\mathbf{u}_t), \tag{7}$$

$$\tau(\mathbf{u}_t) = \mu\left[\nabla\mathbf{u}_t + (\nabla\mathbf{u}_t)^{\mathrm{T}}\right] + \left(\mu_B - \frac{2}{3}\mu\right)(\nabla\cdot\mathbf{u}_t)\mathrm{I}, \tag{8}$$

$$\tau(\mathbf{u}_0) = \mu\left[\nabla\mathbf{u}_0 + (\nabla\mathbf{u}_0)^{\mathrm{T}}\right] + \left(\mu_B - \frac{2}{3}\mu\right)(\nabla\cdot\mathbf{u}_0)\mathrm{I}, \tag{9}$$

where τ, β_T, μ, and μ_B are the viscous stress tensor, the isothermal compressibility, the dynamic viscosity, and the bulk viscosity, respectively. In the linearised Navier-Stokes equation, p_0, $\mathbf{u}_0$, T_0, and ρ_0 are absolute pressure, velocity, temperature, and density of the background mean flow used to account for the effect of the background mean flow on the sound wave. This is calculated by using the CFD study of the fluid.

When the sound waves propagate in the turbulent flow, the flow properties are evaluated by RANS (Reynolds-averaged Navier-Stokes) model (Menter, 1994). The Reynolds-averaged representation of turbulent flow divides the flow quantities into a time-averaged part and a fluctuating part

$$\mathbf{u}_0 = \overline{\mathbf{u}}_0 + \mathbf{u}_0', \quad \rho_0 = \overline{\rho}_0 + \rho_0', \quad p_0 = \overline{p}_0 + p_0'. \tag{10}$$

To discuss the turbulent flow, the SST (Shear Stress Transport) turbulent method is used among various RANS models (Ostashev, Wilson, 2016). The advantage of this method is that it can describe the flow characteristics well close to the wall and the dependence on the initial parameters of the main free stream flow is not very large. Then, the basic equations are defined as:

$$\frac{\partial\overline{\rho}_0}{\partial t} + \nabla\cdot(\overline{\rho}_0\overline{\mathbf{u}}_0) = 0, \tag{11}$$

$$\begin{aligned}\overline{\rho}_0\frac{\partial\overline{\mathbf{u}}_0}{\partial t} + \overline{\rho}_0(\overline{\mathbf{u}}_0\cdot\nabla)\overline{\mathbf{u}}_0 &= \nabla\cdot\Big\{-\overline{p}_0\mathbf{I} + (\mu+\mu_T)\left[\nabla\overline{\mathbf{u}}_0 + (\nabla\overline{\mathbf{u}}_0)^{\mathrm{T}}\right] \\ &\quad -\frac{2}{3}(\mu+\mu_T)(\nabla\cdot\overline{\mathbf{u}}_0)\mathbf{I} - \frac{2}{3}\overline{\rho}_0 k\mathbf{I}\Big\} + \mathbf{F}.\end{aligned} \tag{12}$$

The model equations are formulated with the averaged turbulent kinetic energy k and the specific dissipation rate ω,

$$\begin{aligned}\overline{\rho}_0\frac{\partial k}{\partial t} + \overline{\rho}_0(\overline{\mathbf{u}}_0\cdot\nabla)k &= \nabla\cdot[(\mu+\mu_T\sigma_k)\nabla k] \\ &\quad + P - \overline{\rho}_0\beta_0^* k\omega,\end{aligned} \tag{13}$$

$$\begin{aligned}\overline{\rho}_0\frac{\partial\omega}{\partial t} + \overline{\rho}_0(\overline{\mathbf{u}}_0\cdot\nabla)\omega &= \frac{\overline{\rho}_0\gamma}{\mu_T}P - \overline{\rho}_0\beta\omega^2 \\ &\quad + \nabla\cdot[(\mu+\mu_T\sigma_\omega)\nabla\omega] \\ &\quad + 2(1-f_{v1})\frac{\overline{\rho}_0\sigma_{\omega 2}}{\omega}\nabla\omega\cdot\nabla k,\end{aligned} \tag{14}$$

where

$$P = \min(P_k,\ 10\overline{\rho}_0\beta_0^* k\omega), \tag{15}$$

$$\begin{aligned}P_k &= \mu_T\left\{\nabla\overline{\mathbf{u}}_0 : \left[\nabla\overline{\mathbf{u}}_0 + (\nabla\overline{\mathbf{u}}_0)^{\mathrm{T}}\right] - \frac{2}{3}(\nabla\cdot\overline{\mathbf{u}}_0)^2\right\} \\ &\quad -\frac{2}{3}\overline{\rho}_0 k\nabla\cdot\overline{\mathbf{u}}_0.\end{aligned} \tag{16}$$

In this case, the turbulent eddy viscosity is

$$\mu_T = \frac{\overline{\rho}_0\alpha_1 k}{\max(\alpha_1\omega, Sf_{v2})}, \tag{17}$$

where S is the characteristic magnitude of the mean velocity gradient,

$$S = \sqrt{2S_{ij}S_{ij}}, \tag{18}$$

and S_{ij} is the mean strain rate tensor,

$$S_{ij} = \frac{1}{2}\left(\frac{\partial\overline{u}_{0i}}{\partial x_j} + \frac{\partial\overline{u}_{0j}}{\partial x_i}\right). \tag{19}$$

The constants β, γ, σ_k, and σ_ω are the interpolated values between inner and outer values :

$$\begin{aligned}\beta &= f_{v1}\beta_1 + (1-f_{v1})\beta_2, \\ \gamma &= f_{v1}\gamma_1 + (1-f_{v1})\gamma_2, \\ \sigma_k &= f_{v1}\sigma_{k1} + (1-f_{v1})\sigma_{k2}, \\ \sigma_\omega &= f_{v1}\sigma_{\omega 1} + (1-f_{v1})\sigma_{\omega 2}.\end{aligned} \tag{20}$$

The interpolation functions f_{v1}, f_{v2}, and parameters β_1, β_2, γ_1, γ_2, σ_{k1}, σ_{k2}, σ_{ω_1}, σ_{ω_2}, α_1, and β_0^* are given in (Menter, 1994).

3. Results and analysis

In this section, we first describe the simulation parameters and acoustic characteristic parameters of the acoustic metamaterial to be considered. Additionally, to investigate the effect of the geometrical structure on sound transmission, the sound pressure level characteristic values and transmission loss results are calculated and analysed using finite element simulation in the case of no flow. Next, when there is turbulent flow, the sound transmission properties are investigated according to the change in the flow velocity based on the CFD analysis of the flow, and the effects of convection and eddy are compared with each other. Finally, while changing the geometric structure parameter, we observe the change of sound pressure level and sound transmission loss values.

3.1. Simulation parameters

Figure 1 is a schematic diagram of an acoustic metamaterial consisting of a straight hole through which a fluid can pass and periodic annular cavities surrounding the hole. In Fig. 1, r_a is the radius of the annular cavity, r_d is the radius of the circular duct, t_a is the height of the annular cavity, t_d is a half of the height of the neck in the circular duct, t_s is the height of the acoustic source, and t_p is the height of PML (Perfectly Matched Layer).

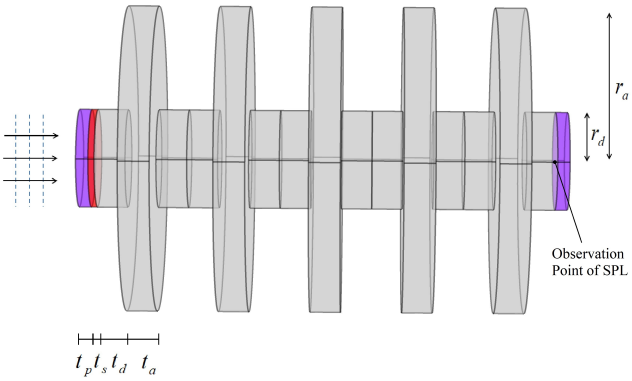

Fig. 1. A schematic diagram of the acoustic metamaterial.

When setting the parameters of acoustic metamaterials, acoustic experiment performed with acrylic metamaterial panels should be considered (Jung *et al.*, 2018). In this experiment, to verify the noise attenuation performance of the acoustic metamaterial panel, the arrays of $96 \times 100 \times 100$ mm containing 6 unit cells were periodically placed on the yz-plane. Then, the power transmission coefficients were measured using four microphones (GRAS 46BE Microphone) and one horn drive (InterM DU-75). Therefore, we set the simulation parameters based on this acoustic experiment. Table 1 shows the values of the other geometrical parameters except for the value of radius r_a because it is calculated while changing r_a to 22.5 mm, 25 mm, 27.5 mm, and 30 mm.

Table 1. Geometric structure parameters.

r_d [mm]	t_a [mm]	t_d [mm]	t_s [mm]	t_p [mm]
8	5	5	1	2

As shown in Fig. 1, the discussed acoustic wave is a plane wave, and its incident surface is perpendicular to the rotation axis direction of the acoustic metamaterial. The finite element simulation was performed with the commercial software COMSOL Multiphysics 5.5. In this case, the boundary condition of the numerical simulation is assumed to be no slip, and the sound velocity is $c_0 = 343$ m/s. PML is applied to the inlet and outlet, which acts to absorb acoustic waves by simulating an open boundary. We calculated the sound pressure in the frequency range of 2000 to 6000 Hz and evaluated the transmission loss and sound pressure level based on it. In this case, the transmission loss of the system is defined as

$$\mathrm{TL} = 20\log_{10}\left(\left|\frac{p_{\mathrm{in}}}{p_{\mathrm{out}}}\right|\right), \tag{21}$$

where p_{in} and p_{out} are the average pressure at the inlet and outlet, respectively (Du *et al.*, 2016; Gikadi *et al.*, 2014). When the sound pressure p changes harmonically with time, SPL (sound pressure level) L_p is expressed by the root mean square pressure p_{rms} of the fluid, such as

$$L_p = 20\log_{10}\left(\frac{p_{\mathrm{rms}}}{p_{\mathrm{ref}}}\right), \qquad p_{\mathrm{rms}} = \sqrt{pp^*/2}, \tag{22}$$

where p_{ref} is the reference pressure for the zero level corresponding to it, and the symbol * indicates the complex conjugate (Pierce, 2019). The zero level corresponding to this dB scale depends on the type of fluid. For example, the reference pressure in air is 20 μPa and the reference pressure in water is 1 μPa.

3.2. Calculation results of sound pressure level in case of no flow

We first investigate the acoustic pressure in the acoustic metamaterial in the case of no flow to evaluate the effect of the geometry on the sound transmission of the acoustic metamaterial with turbulent flow. In this case, an incident acoustic plane wave with an amplitude of 1 Pa is incident in a direction parallel to the axis of rotation of the acoustic metamaterial in the area marked in red in Fig. 1. Since the properties of the sound pressure vary according to the geometric size, we investigated the change in the sound pressure level corresponding to the radius of the annular cavity and the number of annular cavities. The observation point of SPL is shown Fig. 1.

Figure 2a shows the sound pressure level values versus the frequencies of the sound wave when there is no flow (Ma = 0) and the radius of the annular cavity is 22.5 mm. As shown in Fig. 2a, as the frequency increases in the low frequency region, the sound pressure level value decreases rapidly, has a minimum value at a specific frequency (4529.1 Hz in the case of $N = 5$), and then rises again. In other words, it has a resonant property, which can be treated as the result of the interaction between the particle vibration in the direction of sound propagation in the circular duct and the particle vibration perpendicular to the direction of sound propagation in the annular cavity (Jung *et al.*, 2018).

This property appears regardless of the number of annular cavities. However, as the number increases, the magnitude of these minima becomes clearly smaller and the resonance strength becomes stronger. This is because, as the number of annular cavities increases, the cross-region between the particle vibration in the sound propagation direction in the circular duct and the particle vibration perpendicular to the sound propagation direction in the annular cavity increases, and as a result, the interaction becomes stronger. In the case of $N = 1$, another peak appears at 3293.8 Hz. Its peak intensity is smaller than the peak discussed earlier, and it gets weaker as the number of annular cavities increases. This is a peak related to the length of the circular duct. In the case of $N = 1$, this peak cannot be ignored because the resonance related to the interaction is not very large. However, as the number of annular cavities increases, the interaction between the particle vibration in the direction of sound propagation in the circular duct and the particle vibration perpendicular to the direction of sound propagation in the annular cavity increases, and the intensity of this peak disappears.

Even when r_a is 25.0 mm, 27.5 mm, and 30.0 mm, the resonance properties analysed above still appear (Figs 2b–2d). Table 2 shows the resonant frequency values corresponding to the annular cavity radii in the case of $N = 5$. Note in Fig. 2 and Table 2 that the reso-

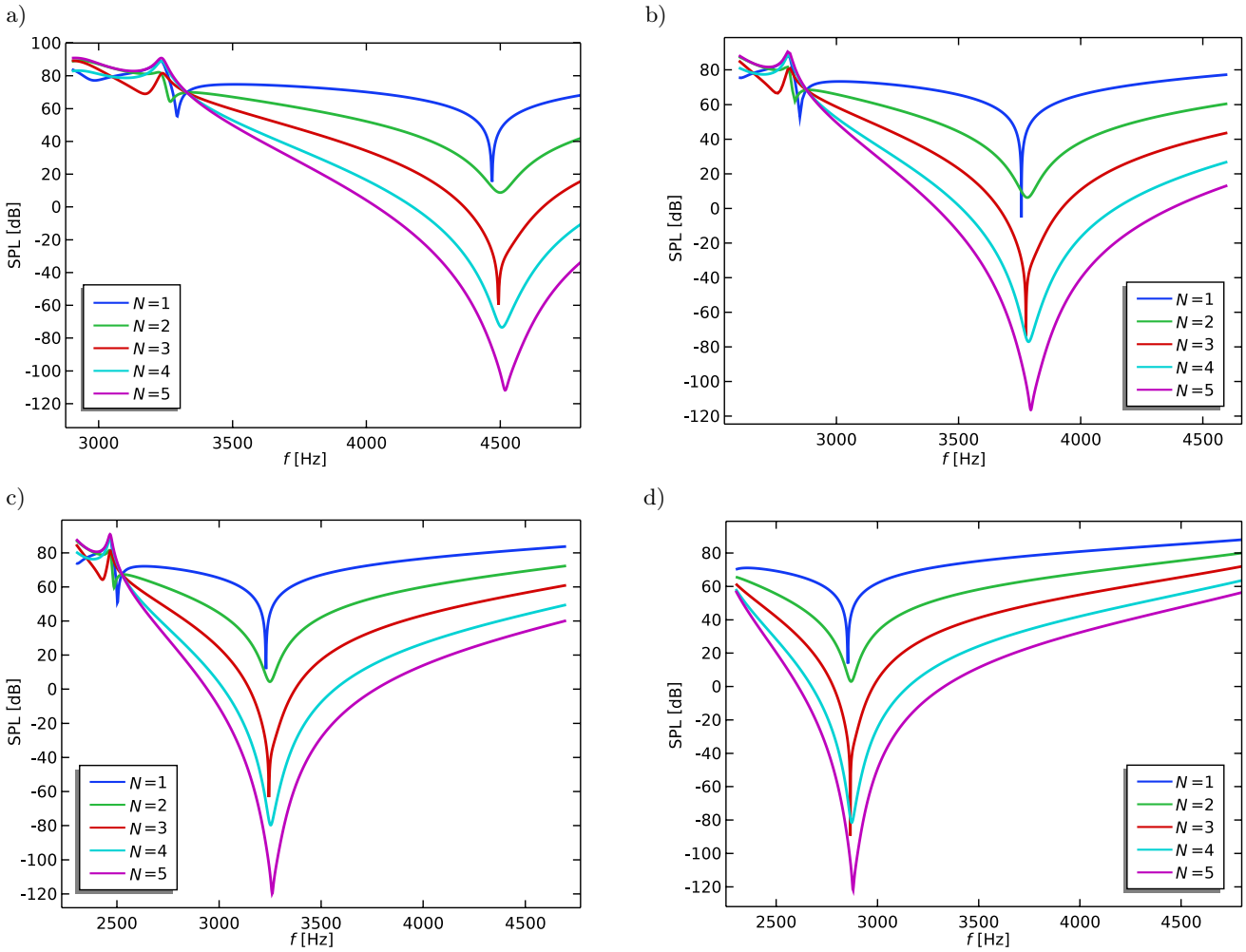

Fig. 2. In the case of no flow, the dependence of the SPL on frequency for different radii of the annular cavity and the number of annular cavities; the observation point of SPL is shown in Fig. 1: a) r_a = 22.5 mm, Ma = 0, b) r_a = 25.0 mm, Ma = 0, c) r_a = 27.5 mm, Ma = 0, d) r_a = 30.0 mm, Ma = 0.

nant frequency decreases as the radius of the annular cavity increases. This is analysed with particle vibrations perpendicular to the direction of sound propagation in the annular cavity. As the radius of the annular cavity increases, the wavelength of the stationary wave in the cavity increases, and thus the resonance frequency decreases. As a result, the resonance frequency of the sound propagation is also lowered due to the interaction between the particle vibration in the sound propagation direction in the circular duct and the particle vibration perpendicular to the sound propagation direction in the annular cavity. This proves once again that this resonance property is closely related to the particle vibration in the annular cavity.

Table 2. Resonant frequency values corresponding to the radii of the annular cavity in the case of $N = 5$.

r_a [mm]	22.5	25.0	27.5	30.0
f^{res} [Hz]	4529.1	3804.8	3267.6	2862.3

3.3. CFD analysis of turbulent flow

To investigate the sound propagation properties of the acoustic metamaterials with turbulent flow, CFD analysis of turbulence in airflow is performed using the SST model mentioned above. The velocity of turbulent flow is evaluated with the Mach number Ma, and the properties of the case where Ma is 0.02, 0.05, 0.10, 0.15, 0.17, 0.20, 0.22 are discussed. In this case, the kinematic viscosity of air is $\nu = 1.50 \cdot 10^{-5}$ m^2/s.

The investigation of turbulent flow is determined through the evaluation and analysis of the turbulent kinetic energy, specific dissipation rate, turbulent dissipation rate, turbulent dynamic viscosity, turbulent kinematic viscosity, and turbulence time scale. Table 3 shows the turbulent flow parameters obtained at the outlet of the acoustic metamaterial by running the simulation according to the change in the velocity of the turbulent flow. As Ma increases, the turbulent kinetic energy, specific dissipation rate, turbulent dissipation rate, turbulent dynamic viscosity, and turbulent kinematic viscosity increase. However, as Ma increases, the turbulence time scale decreases, which is in good agreement with the fact that τ_T is inversely proportional to the specific dissipation rate ω. Figure 3 shows a quarter cross-section of turbulent dynamic viscosity μ_T in the case of Ma = 0.15. It is evident that the turbulent dynamic viscosity is not zero in the annular cavity region of Fig. 3, and this fact intuitively shows that the annular cavity region has a great influence on the airflow flowing through the circular duct.

Table 3. Turbulent flow parameters at the outlet of the acoustic metamaterials.

Ma	0.02	0.05	0.10	0.15	0.17	0.20	0.22
k [m^2/s^2]	0.00538	0.225	3.86	14.6	21.1	33.3	43.0
ω [10^5 s^{-1}]	8.92	8.94	9.25	10.1	10.5	11.3	11.9
ε [10^4 m^2/s^3]	0.0432	1.81	32.1	132	199	338	461
μ_T [10^{-7} Pa·s]	0.0727	3.03	50.2	175	242	355	436
ν_T [10^{-7} m^2/s]	0.0603	2.52	41.7	145	201	294	361
τ_T [10^{-5} s]	1.25	1.24	1.20	1.11	1.06	0.983	0.933

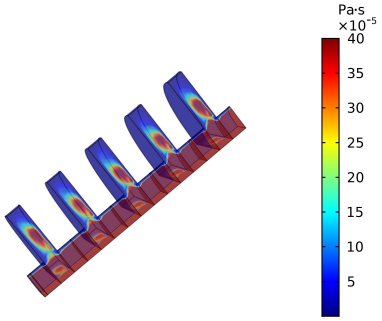

Fig. 3. A quarter cross-section of the turbulent dynamic viscosity in the case of Ma = 0.15.

It is important to evaluate the property of the turbulent dissipation rate ε in investigating the turbulent flow of a fluid. The turbulent dissipation rate ε does not depend on the kinematic viscosity ν, but instead is determined by the nature of the largest eddy that extracts energy from the mean flow (Kundu *et al.*, 2012). A scale that well reflects the balance between the inertia effect and the viscous effect of eddy is Kolmogorov's scale, defined as

$$\eta = (\nu^3/\varepsilon)^{1/4}. \tag{23}$$

Therefore, it is necessary to consider this scale carefully to evaluate the properties of turbulent flow and to analyse the sound transmission result accurately in turbulent flow. Thus, we investigated the Kolmogorov's scale versus the velocity of air (Fig. 4). As shown in Fig. 4, as Ma increases, Kolmogorov's scale gradually decreases. That is, the faster the velocity, the smaller the effect of eddy. In Fig. 4, the scale was also evaluated according

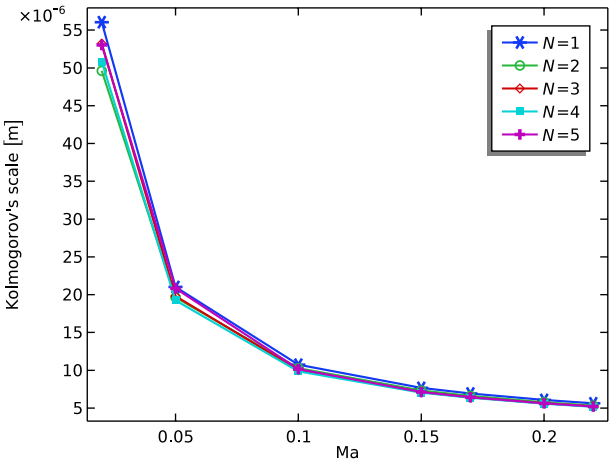

Fig. 4. Kolmogorov's scale versus the velocity of airflow.

to the number of the annular cavities, but there is no significant change depending on the number.

3.4. Sound transmission in turbulent flow

We investigated the transmission properties of sound waves in turbulent flow with the linearised Navier-Stokes Model discussed in Sec. 2, based on determining the pressure, velocity, temperature, and density of turbulent flow in the acoustic metamaterials. In this case, the incident acoustic plane wave of $p_b = p_0 e^{-ik_0 z}$ is incident on the area marked in red in Fig. 1 in a direction perpendicular to the rotation axis of the acoustic metamaterial, where $p_0 = 1$ Pa, $k_0 = \omega_0/[c_0(\mathrm{Ma}+1)]$. In this case, ω_0 is the angular frequencies of the incident acoustic wave.

Figure 5 shows a quarter cross-section of the acoustic pressure obtained as a simulation result for $f = 5700$ Hz, Ma = 0.15, and $r_a = 25$ mm. From this figure, it can be seen that even in the turbulent flow, the sound transmission can be relatively blocked due to the geometry of the acoustic metamaterials. Thus, we investigated the sound transmission loss while increasing the flow velocity.

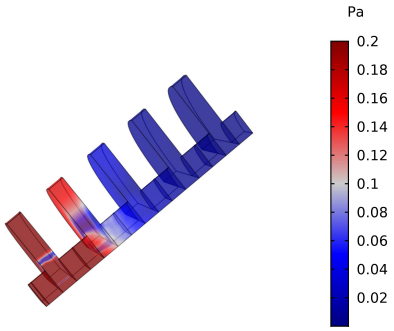

Fig. 5. A quarter cross-section of the acoustic pressure in the case of $f = 5700$ Hz, Ma = 0.15, and $r_a = 25$ mm.

Figures 6 and 7 show the sound transmission loss results calculated while changing the value of Ma and

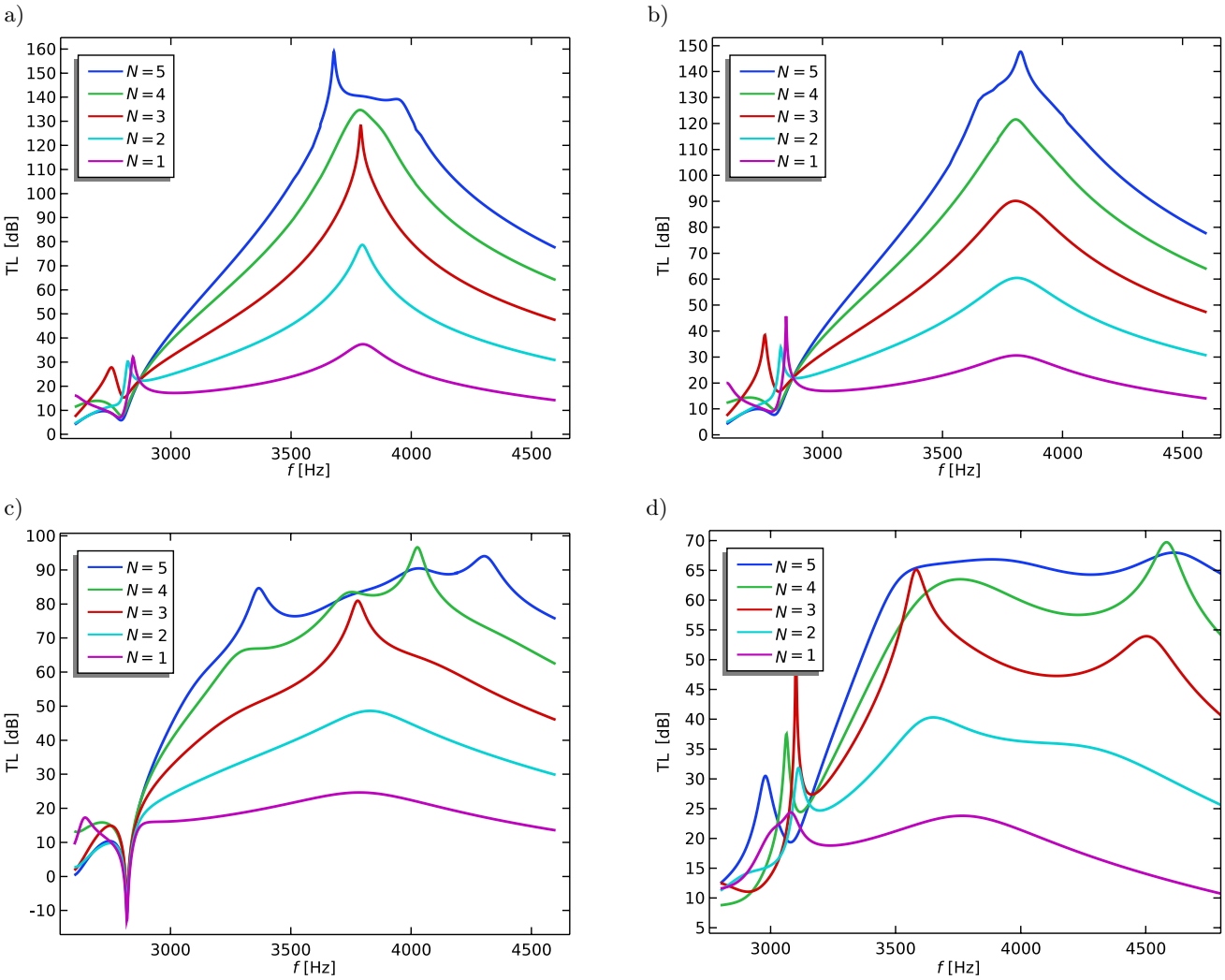

Fig. 6. Dependence of sound transmission loss for different values of Ma and numbers of annular cavities with $r_a = 25$ mm in the case of Ma = 0.02, 0.05, 0.10, and 0.15: a) Ma = 0.02, $N = 5$, b) Ma = 0.05, $N = 5$, c) Ma = 0.10, $N = 5$, d) Ma = 0.15, $N = 5$.

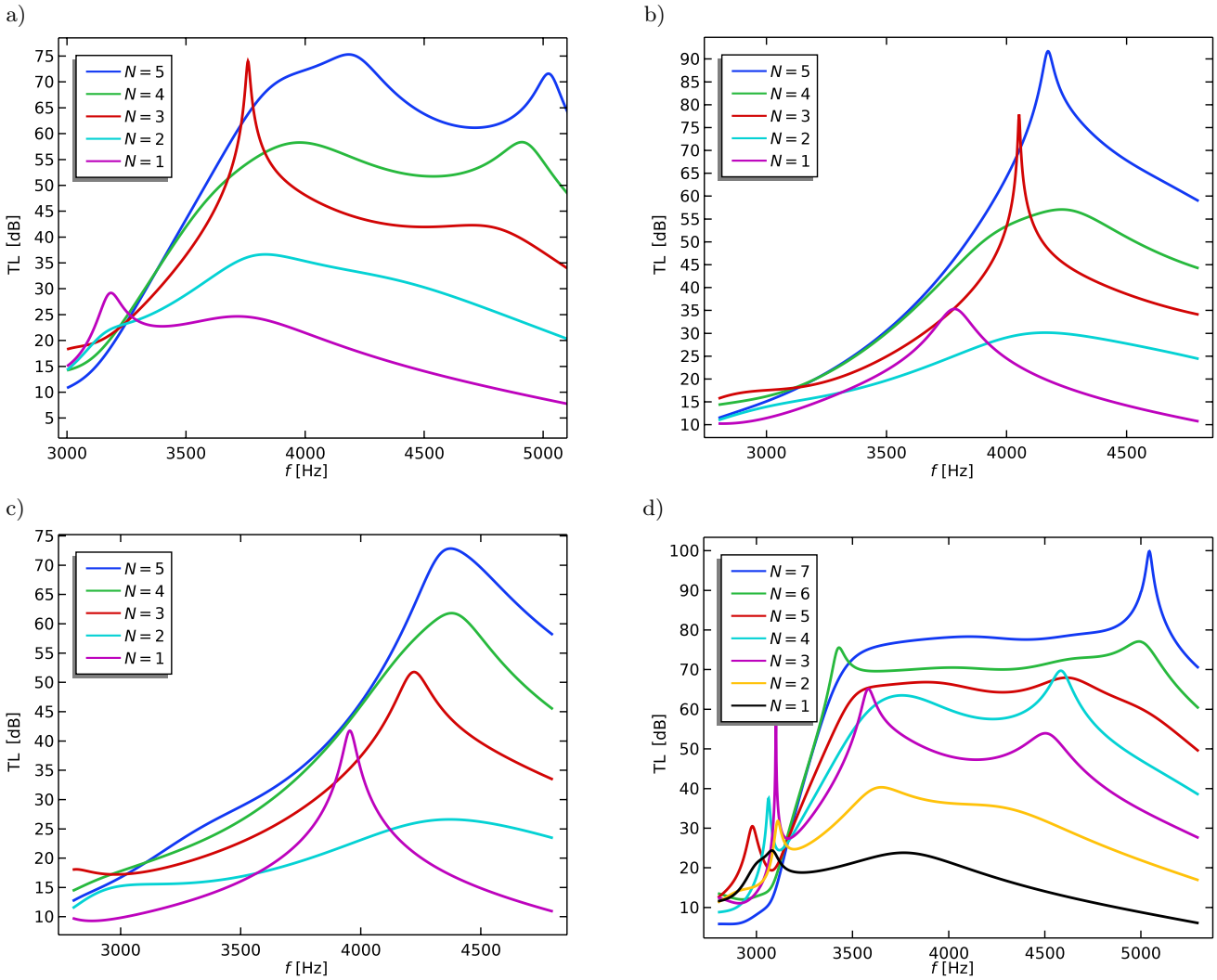

Fig. 7. Dependence of sound transmission loss for different values of Ma and numbers of annular cavities with r_a = 25 mm in the case of Ma = 0.17, 0.20, and 0.22: a) Ma = 0.17, N = 5, b) Ma = 0.10, N = 5, c) Ma = 0.22, N = 5, d) Ma = 0.15, N = 7.

the number of annular cavities in the case of r_a = 25 mm. To evaluate the sound transmission loss corresponding to the flow velocity and the number of annular cavities in detail, the number of annular cavities was changed from 1 to 5 and the size of Ma was changed from 0.02 to 0.22 in Figs 6 and 7a–7c. In addition, a detailed calculation of the transmission loss is shown while changing the number of annular cavities from 1 to 7 in the case of Ma = 0.15 in Fig. 7d.

In the case of Ma = 0 and r_a = 25 mm, the resonant frequency is 3804.8 Hz. If one analyses Fig. 6a in detail, one can see that the resonant frequency is rather lower than when there is no flow. In this case, since Ma = 0.02, the convective velocity is small, on the contrary, the Kolomogorov's scale is very large (see Fig. 4). Therefore, the effect of eddy is greater than the effect of convective velocity on sound in this case. The fact that the resonance frequency of the case of $N = 1, 2, 3, 4$ in Fig. 6a is lower than that of the case of no flow shows that the effect of eddy shifts the resonance frequency to a lower frequency. Since the eddy generates a flow opposite to the direction of the convection, considering the Doppler effect, it is obvious that the resonant frequency moves to the lower frequency range due to the effect of the eddy.

Additionaly, the figure reflects the fact that when N increases, the intrinsic interaction of the acoustic metamaterials becomes stronger and the peak intensity gradually increases. In the case of N = 5, the sound transmission loss values are different from the above case. The value change from the first peak of 3677.9 Hz to the second peak of 3938 Hz becomes gentle, and as a result, the widening property of the resonance peak appears. In the case of N = 5, the number of annular cavities increases compared to the case of $N = 1, 2, 3, 4$. Therefore, the interaction between the particle vibration in the sound propagation direction in the circular duct and the particle vibration perpendicular to the

sound propagation direction in the annular cavity becomes strong. In this case, not only the effect of eddy, but also the intrinsic interaction of the acoustic metamaterials has a considerable influence on the sound propagation. Of course, the fact that the largest peak frequency of the figure has been lowered to 3677.9 Hz shows that the eddy effect still plays a large role at this time. However, the newly revealed widening properties in the figure reflect that the intrinsic interaction of the acoustic metamaterials has a significant effect on sound propagation. In the case of Fig. 6b, the effect of convection in the case of Ma > 0.02 is larger than that in the case of Ma = 0.02. This can be known well by seeing that the peak frequency shifted to 3824.7 Hz in the case of Ma = 0.05 and N = 5. However, the widening property of this case is not significantly different from that of the case of Ma = 0.02. In the case of Fig. 6c, the effect of convection becomes stronger, and the widening property appears at $N \geq 4$. In the case of Ma = 0.15 and Ma = 0.17, the effect of intrinsic interaction due to the geometry of the acoustic metamaterial, the effect of convection, and the effect of eddy become similar. As a result, the widening property appears at $N \geq 1$ in Figs 6d and 7a. However, the effect of convection becomes larger in the case of Ma = 0.17 than in the case of Ma = 0.15, and the peak is shifted to a larger frequency region in the case of Ma = 0.17 than in the case of Ma = 0.15. When Ma is continuously increased to 0.20 and 0.22, the effect of convection is much larger than that of eddy and the intrinsic interaction of acoustic metamaterials, so there is no widening property and the peak moves to a larger frequency range (Figs 7b and 7c). Figure 7d is a graph that investigates the sound transmission loss while increasing the number of annular cavities in the velocity range of Ma = 0.15, where the three interactions are similar. Figure 7d shows that in the case of Ma = 0.15, the geometric interaction effect of the acoustic metamaterial begins to play an important role only when N is 7 or more.

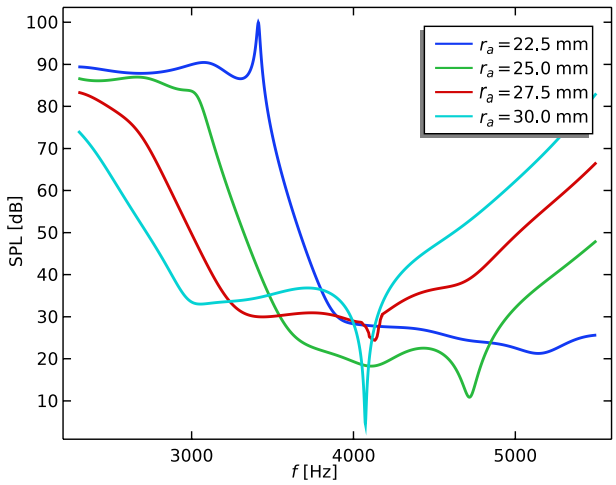

Fig. 8. In the case of Ma = 0.15, the result of the sound pressure level according to the increase of the annular cavity radius.

Figure 8 shows the result of the sound pressure level according to the increase of the annular cavity radius in the case of Ma = 0.15. In this case, it is affected by convection and eddy, but similar to the case of Ma = 0, as the radius increases, the resonance frequency of the sound pressure level decreases. This fact shows that the particle vibration in the annular cavity analysed in the case of Ma = 0 is a mechanism that cannot be ignored even in the acoustic propagation analysis in turbulent flow.

4. Conclusion

In this study, we discussed the influence of the geometric structure, convection, and eddy on sound propagation in the acoustic metamaterials with turbulent flow. First, to evaluate the influence of the geometric structure, the acoustic pressure in the acoustic metamaterial was investigated in the case of no flow. Looking at the sound pressure levels corresponding to the frequencies of the sound wave, it has resonance properties. Furthermore, the more the number of annular cavities increases, the larger resonance peak gets. In addition, as the radius of the annular cavity increases, the resonant frequency decreases. This shows that the sound propagation properties of the acoustic metamaterials are closely related to the geometry.

To discuss the problem of sound propagation into turbulent flow in the acoustic metamaterial, not only the effect of convection and eddy, but also the effect of the intrinsic interactions reflecting the geometric structure of the acoustic metamaterial must be considered. Here, the intrinsic interaction refers to the interaction between the particle vibration in the sound propagation direction in the circular duct and the particle vibration perpendicular to the sound propagation direction in the annular cavity. It is not an easy matter to interpret this because all three effects contribute to sound transmission. Of course, both the effects of convection and eddy reduce the intrinsic interaction of the acoustic metamaterials in the circular duct, thus reducing the resonant peak intensity for sound transmission. However, considering that the direction of convection is the same as the direction of sound propagation and the direction of eddy is opposite to the direction of sound propagation, the effect of convection is opposite to the effect of eddy. In other words, the effect of convection causes the resonance peak to move to the higher frequency region, and the effect of eddy causes the resonance peak to move to the lower frequency region.

However, when these are combined with the unique interaction properties of the acoustic metamaterials, the widening property of the resonance peak appears. In short, when all three effects cannot be ig-

nored, competition phenomena appear, and as a result, the resonance peak widens and the intensity decreases. In this respect, it is different from the result of Jung *et al.* (2018). Because turbulent flow was not considered, the shift of the resonant frequency and the widening property of the resonant peak did not appear in their result. In conclusion, the effects of convection, eddy, and intrinsic interactions arising from the unique geometry of acoustic metamaterials appear as the shift of the resonant frequency and the widening properties of the resonant peak.

By using the shift of the resonant frequency and the widening property of the resonant peak studied here, it is possible to block the noise by properly controlling the geometric size and shape of the acoustic metamaterials even if the turbulent flow exists. In particular, this can be used to block noise in transport systems such as trains, cars, and ships.

In practical applications, there are instabilities in the flow (e.g. Kelvin-Helmholtz instability), which lead to turbulent flow. Therefore, the problem for elucidating the acoustic properties of acoustic metamaterials in turbulent flows becomes a practical problem (e.g. ventilations shafts). Additionally, this becomes an important problem in the application of acoustic metamaterials to aeroacoustics. Our results will be applied to the acoustic absorption and dissipation, noise trapping, and acoustic cloaking.

Acknowledgments

It is a pleasure to thank Un Chol Ri, Yong Kwang Jong, and Chol Su Ri for useful discussions. This work was supported by the National Program on Key Science Research of Democratic People's Republic of Korea (Grant No. 20-15-5).

References

1. Ananthan V., Bernicke P., Akkermans R., Hu T., Liu P. (2020), Effect of porous material on trailing edge sound sources of a lifting airfoil by zonal oversetles, *Journal of Sound and Vibration*, **480**: 115386, doi: 10.1016/j.jsv.2020.115386.
2. Bok E., Park J.J., Choi H., Han C.K., Wright O.B., Lee S.H. (2018), Metasurface for water-to-air sound transmission, *Physical Review Letters*, **120**(4): 044302, doi: 10.1103/PhysRevLett.120.044302.
3. Brookea D.C., Umnova O., Leclaire P., Dupont T. (2020), Acoustic metamaterial for low frequency sound absorption in linear and nonlinear regimes, *Journal of Sound and Vibration*, **485**: 115585, doi: 10.1016/j.jsv.2020.115585.
4. Carpio A.R., Avallone F., Ragni D., Snellen M., van der Zwaag S. (2019), Mechanisms of broadband noise generation on metal foam edges, *Physics of Fluids*, **31**(10): 105110, doi: 10.1063/1.5121248.
5. Chaitanya P., Joseph P., Ayton L.J. (2020), Leading edge profiles for the reduction of airfoil interaction noise, *AIAA Journal*, **58**(3): 1118–1129, doi: 10.2514/1.J058456.
6. Deuse M., Sandberg R.D. (2020), Different noise generation mechanisms of a controlled diffusion aerofoil and their dependence on Mach number, *Journal of Sound and Vibration*, **476**: 115317, doi: 10.1016/j.jsv.2020.115317.
7. Du L., Holmberg A., Karlsson M., Åbom M. (2016), Sound amplification at a rectangular t-junction with merging mean flows, *Journal of Sound and Vibration*, **367**: 69–83, doi: 10.1016/j.jsv.2015.12.042.
8. Fan L., Chen Z., Zhang S., Ding J., Li X., Zhang H. (2015), An acoustic metamaterial composed of multi-layer membrane-coated perforated plates for low-frequency sound insulation, *Applied Physics Letters*, **106**(15): 151908, doi: 10.1063/1.4918374.
9. Gikadi J., Föller S., Sattelmayer T. (2014), Impact of turbulence on the prediction of linear aeroacoustic interactions: Acoustic response of a turbulent shear layer, *Journal of Sound and Vibration*, **333**(24): 6548–6559, doi: 10.1016/j.jsv.2014.06.033.
10. Gu Z., Gao H., Liu T., Li Y., Zhu J. (2020), Dopant-modulated sound transmission with zero index acoustic metamaterials, *The Journal of the Acoustical Society of America*, **148**(3): 1636–1641, doi: 10.1121/10.0001962.
11. Jiang X., Li Y., Zhang L.K. (2017), Thermoviscous effects on sound transmission through a metasurface of hybrid resonances, *The Journal of the Acoustical Society of America*, **141**(4): EL363–EL368, doi: 10.1121/1.4979682.
12. Jung J.W., Kim J.E., Lee J.W. (2018), Acoustic metamaterial panel for both uid passage and broadband soundproofing in the audible frequency range, *Applied Physics Letters*, **112**(4): 041903, doi: 10.1063/1.5004605.
13. Kundu P.K., Cohen I.M., Dowling D. (2012), *Fluid mechanics*, 5th ed., pp. 564–571, Elsevier, doi: 10.1016/C2009-0-63410-3.
14. Kusano K., Yamada K., Furukawa M. (2020), Aeroacoustic simulation of broadband sound generated from low-Mach-number flows using a lattice Boltzmann method, *Journal of Sound and Vibration*, **467**: 115044, doi: 10.1016/j.jsv.2019.115044.
15. Li Y., Assouar B.M. (2016), Acoustic metasurface-based perfect absorber with deep subwavelength thickness, *Applied Physics Letters*, **108**(6): 063502, doi: 10.1063/1.4941338.
16. Lu K., Wu J., Guan D., Gao N., Jing L. (2016), A lightweight low-frequency sound insulation membrane-type acoustic metamaterial, *AIP Advances*, **6**(2): 025116, doi: 10.1063/1.4942513.
17. Menter F. (1994), Two-equation eddy-viscosity turbulence models for engineering applications, *AIAA Journal*, **32**(8): 1598–1605, doi: 10.2514/3.12149.

18. Nardini M., Sandberg R.D., Schlanderer S.C. (2020), Computational study of the effect of structural compliance on the noise radiated from an elastic trailing-edge, *Journal of Sound and Vibration*, **485**: 115533, doi: 10.1016/j.jsv.2020.115533.

19. Ostashev V.E., Wilson D.K. (2016), *Acoustics in Moving Inhomogeneous Media*, 2ed., pp. 27–62, Taylor and Francis, doi: 10.1201/b18922.

20. Park J.J., Park C.M., Lee K.J., Lee S.H. (2015), Acoustic superlens using membrane-based metamaterials, *Applied Physics Letters*, **106**(5): 051901, doi: 10.1063/1.4907634.

21. Pierce A.D. (2019), *Acoustics: An Introduction to Its Physical Principles and Applications*, 3rd ed., pp. 68–70, Springer, doi: 10.1007/978-3-030-11214-1.

22. Qu S., Sheng P. (2020), Minimizing indoor sound energy with tunable metamaterial surfaces, *Physical Review Applied*, **14**(3): 034060, doi: 10.1103/PhysRev Applied.14.034060.

23. Romani G., Ye Q.Q., Avallone F., Ragni D., Casalino D. (2020), Numerical analysis of fan noise for the NOVA boundary-layer ingestion configuration, *Aerospace Science and Technology*, **96**: 105532, doi: 10.1016/j.ast.2019.105532.

24. Su H., Zhou X., Xu X., Hu G. (2014), Experimental study on acoustic subwavelength imaging of holey-structured metamaterials by resonant tunnelling, *The Journal of the Acoustical Society of America*, **135**(4): 1686–1691, doi: 10.1121/1.4868395.

25. Sui N., Yan X., Huang T.Y., Xu J., Yuan F.G., Jing Y. (2015), A lightweight yet sound-proof honeycomb acoustic metamaterial, *Applied Physics Letters*, **106**(17): 171905, doi: 10.1063/1.4919235.

26. Szőke M., Fiscaletti D., Azarpeyvand M. (2018), Effect of inclined transverse jets on trailing-edge noise generation, *Physics of Fluids*, **30**(8): 085110, doi: 10.1063/1.5044380.

27. Szőke M., Fiscaletti D., Azarpeyvand M. (2020), Uniform flow injection into a turbulent boundary layer for trailing edge noise reduction, *Physics of Fluids*, **32**(8): 085104, doi: 10.1063/5.0013461.

28. Tang H., Lei Y.L., Li X.Z. (2019), An acoustic source model for applications in low Mach number turbulent flows, such as a large-scale wind turbine blade, *Energies*, **12**(23): 4596, doi: 10.3390/en12234596.

29. Wang X., Zhao H., Luo X., Huang Z. (2016), Membrane-constrained acoustic metamaterials for low frequency sound insulation, *Applied Physics Letters*, **108**(4): 041905, doi: 10.1063/1.4940717.

30. Wang Y., Thompson D., Hu Z. (2019), Effect of wall proximity on the flow over a cube and the implications for the noise emitted, *Physics of Fluids*, **31**(7): 077101, doi: 10.1063/1.5096072.

31. Yang Z.J. *et al.* (2015), Topological acoustics, *Physical Review Letters*, **114**(11): 114301, doi: 10.1103/Phys RevLett.114.114301.

32. Yao H., Davidson L. (2019), Vibro-acoustics response of a simplified glass window excited by the turbulent wake of a quarter-spherocylinder body, *The Journal of the Acoustical Society of America*, **145**(5): 3163–3176, doi: 10.1121/1.5109548.

33. Zheng M.Y., Park C., Liu X.N., Zhu R., Hu G.K., Kim Y.Y. (2020), Non-resonant metasurface for broadband elastic wave mode splitting, *Applied Physics Letters*, **116**(17): 171903, doi: 10.1063/ 5.0005408.